

Crystallization of amorphous NiTi shape memory alloy fabricated by severe plastic deformation

Shu-yong JIANG¹, Ming TANG¹, Ya-nan ZHAO¹, Li HU², Yan-qiu ZHANG¹, Yu-long LIANG²

1. Industrial Training Centre, Harbin Engineering University, Harbin 150001, China;

2. College of Materials Science and Chemical Engineering, Harbin Engineering University, Harbin 150001, China

Received 1 July 2013; accepted 3 October 2013

Abstract: Based on the local canning compression, severe plastic deformation (SPD) is able to lead to the almost complete amorphous nickel–titanium shape memory alloy (NiTi SMA), in which a small amount of retained nanocrystalline phase is embedded in the amorphous matrix. Crystallization of amorphous NiTi alloy annealed at 573, 723 and 873 K was investigated, respectively. The crystallization kinetics of the amorphous NiTi alloy can be mathematically described by the Johnson–Mehl–Avrami–Kolmogorov (JMAK) equation. NiTi SMA with a complete nanocrystalline phase is obtained in the case of annealing at 573 K and 723 K, where martensite phase transformation is suppressed due to the constraint of the grain boundaries. Crystallization of amorphous NiTi alloy at 873 K leads to the coarse-grained NiTi sample, where (001) martensite compound twin is observed at room temperature. It can be found that the martensitic twins preferentially nucleate at the grain boundary and they grow up towards the two different grains. SPD based on the local canning compression and subsequent annealing provides a new approach to obtain the nanocrystalline NiTi SMA.

Key words: NiTi alloy; shape memory alloy; severe plastic deformation; amorphization; crystallization

1 Introduction

Nickel–titanium shape memory alloy (NiTi SMA) is widely used in engineering fields because of its shape memory effect as well as superelasticity [1,2]. Cold working plays an important role in engineering application of NiTi SMA and has a significant influence on shape memory effect as well as superelasticity of NiTi SMA [3,4]. However, severe plastic deformation (SPD) based on the cold working is able to lead to nanocrystallization or amorphization of NiTi SMA. So far, plenty of work with respect to SPD of NiTi SMA in the case of cold working has been done over the last decade by means of high pressure torsion (HPT) [5,6], cold rolling [7,8] and cold drawing [9,10]. SPD of NiTi SMA followed by subsequently appropriate heat treatment contributes to improving the mechanical properties and the functional properties of NiTi SMA, such as the high ultimate strength and the high elongation at the elevated temperatures [11] and the perfect superelasticity [12,13], which is attributed to

nanocrystallization of amorphous NiTi SMA prepared by SPD in the case of annealing. Many researchers investigated the crystallization mechanism of amorphous NiTi SMA obtained by SPD and the phase transformation behavior of NiTi SMA after crystallization. NAKAYAMA et al [14] investigated the influence of the annealing on NiTi SMA subjected to cold rolling and found that the martensitic phase transformation temperatures are suppressed by the introduction of elastic strain, lattice defects and crystal refinement. WAITZ et al [15,16] studied martensitic phase transformation behavior in the nanocrystalline NiTi SMA formed as a result of the crystallization of the amorphous structure resulting from HPT and revealed that the grain size has a significant influence on martensitic phase transformation and the (001) compound twins occur frequently in the nanocrystalline NiTi SMA along with martensitic phase transformation. SRIVASTAVA et al [17] revealed that crystallization of the amorphous NiTi alloy as-formed by cold rolling is attributed to the retained nanocrystalline debris acting as the heterogeneous nucleation sites, which leads to high

nucleation rates and low thermal stabilities of the amorphous phase. PETERLECHNER et al [18] investigated the crystallization kinetics of the amorphous NiTi alloy derived from repeated cold rolling and revealed that the crystallization kinetics is consistent with the mixed nucleation or the nucleation with decreasing rate and three-dimensional growth.

In the present study, as a new attempt, SPD based on local canning compression was used for preparing the amorphous NiTi SMA. On the basis of previous study on the influence of annealing on NiTi sample subjected to SPD [19], crystallization of the corresponding amorphous NiTi sample was further investigated at different annealing temperatures.

2 Experimental

The as-drawn NiTi bar with a diameter of 12 mm possesses a nominal composition of Ni_{50.9}Ti_{49.1} (mole fraction, %). According to differential scanning calorimetry (DSC), the transformation temperatures of the NiTi bar are as follows: $M_s=245.8$ K, $M_f=231.3$ K, $A_s=255.7$ K, $A_f=268.9$ K. Therefore, the as-drawn NiTi bar belongs to *B2* austenite structure. The NiTi samples with diameter of 4 mm and height of 6 mm were cut from the NiTi bar by means of electro-discharge machining (EDM) and then were locally inserted into the low carbon steel cans with inner diameter of 4 mm, wall thickness of 3 mm and height of 3 mm. The locally canned NiTi samples were placed between the top anvil and the bottom one of the Instron equipment and then were compressed to the reduction in height by 75% in order to form the amorphous structure, as shown in Fig. 1. The compressed NiTi specimens were annealed at 573, 723 and 873 K for 2 h, respectively, and subsequently were cooled to room temperature in the atmosphere.

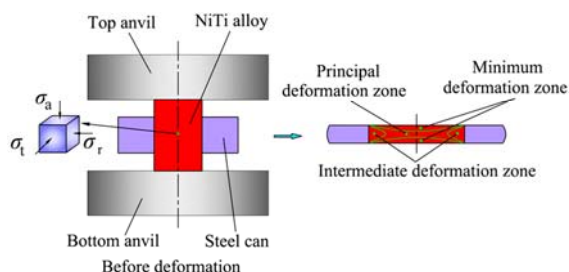


Fig. 1 Schematic diagram of NiTi alloy under local canning compression (σ_a —Axial stress; σ_r —Radial stress; σ_t —Tangential stress)

Microstructural evolution of the NiTi specimens subjected to annealing was characterized by transmission electron microscopy (TEM). Foils for TEM observation were mechanically ground to 70 μm and then thinned by

twin-jet polishing in an electrolyte consisting of 6% HClO₄, 34% C₄H₁₀O and 60% CH₃OH in volume fraction. TEM observations were conducted on a FEI TECNAI G2 F30 microscope with a side-entry and double-tilt sample stage with angular ranges of $\pm 40^\circ$ at an accelerating voltage of 300 kV. High resolution transmission electron microscopy (HRTEM) was also conducted in order to investigate the atomic structure of the NiTi samples subjected to SPD.

3 Results

3.1 Microstructures of as-received NiTi sample

Figure 2 shows TEM image of the as-drawn NiTi bar and the corresponding selected area electron diffraction (SAED) pattern. It can be seen from Fig. 2 that the original NiTi sample consists of coarse grains with *B2* austenite structure.

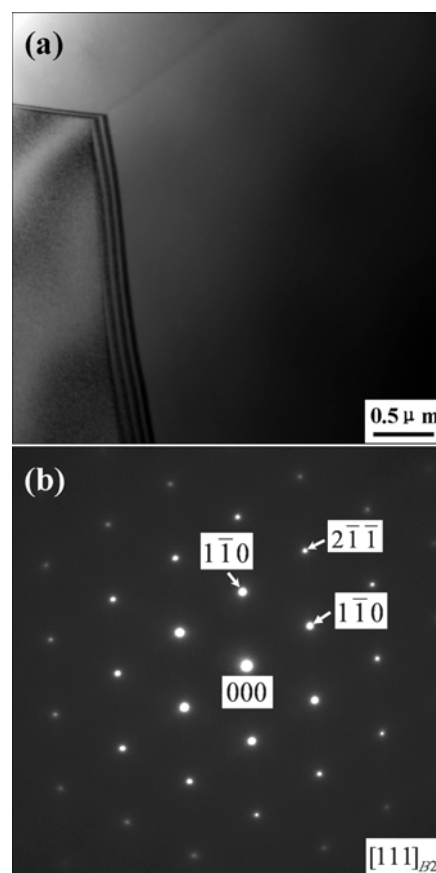


Fig. 2 Microstructure of as-drawn NiTi bar: (a) TEM image; (b) SAED pattern showing *B2* austenite matrix

3.2 Microstructures of NiTi sample subjected to SPD

Figure 3 demonstrates TEM images, SAED pattern, HRTEM image and the corresponding fast Fourier transform (FFT) of NiTi sample at the reduction in height by 75%. It can be seen from Fig. 3 that large plastic deformation leads to an almost complete amorphous phase in which an extremely small amount of

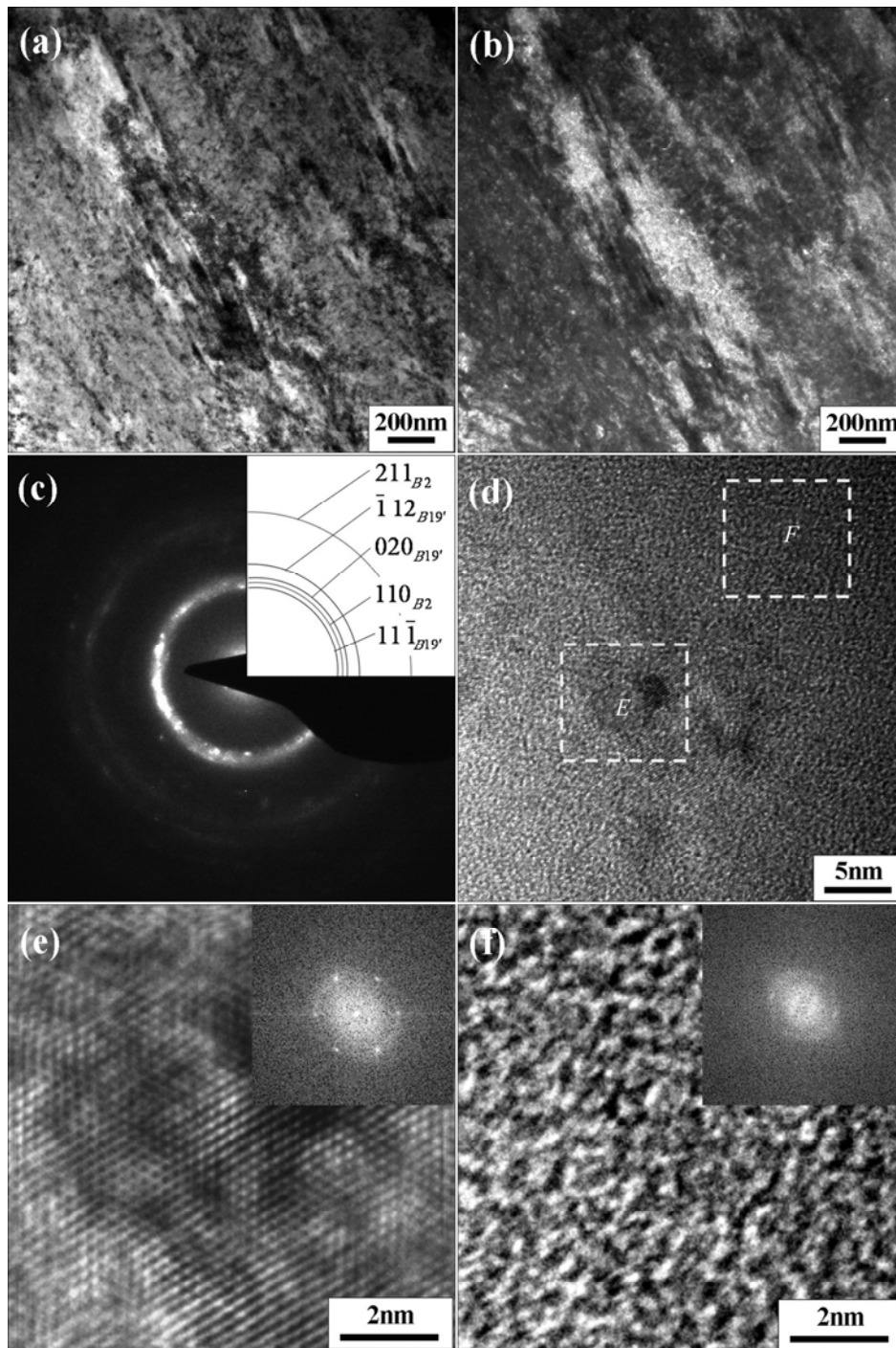


Fig. 3 NiTi sample subjected to SPD at reduction in height by 75%: (a) TEM bright field image; (b) TEM dark field image; (c) SAED pattern showing presence of amorphous diffraction ring and nanocrystalline diffraction ring; (d) HRTEM image showing almost complete amorphous phase; (e) FFT of zone *E* in (d) showing nanocrystalline phase; (f) FFT of zone *F* in (d) showing amorphous phase

nanocrystalline phase is embedded in the amorphous NiTi matrix. Furthermore, the *B2* austenite phase and the *B19'* martensite phase coexist in the retained nanocrystalline debris, which reveals that SPD leads to the occurrence of stress-induced martensite phase transformation and thus it contributes to mechanical stabilization of stress-induced martensite. In addition, the retained nanocrystalline phase exhibits more lattice

defects and the atomic arrangement in the amorphous phase is characterized by a complete disorder, as shown in Figs. 3 (e) and (f).

3.3 Microstructures of amorphous NiTi sample after annealing at 573 K

Figure 4 indicates the TEM photograph and the corresponding SAED pattern of microstructure of the

NiTi sample subjected to SPD as well as subsequent annealing at 573 K for 2 h. It can be clearly seen from Fig. 4 that annealing at 573 K for 2 h results in the complete nanocrystallization of the amorphous NiTi sample derived from SPD. The homogenous nanocrystalline structures with different grain sizes in the NiTi sample are obtained and the mean grain size is about 12 nm. The SAED pattern indicates that the nanocrystalline NiTi sample completely belongs to $B2$ austenite structure.

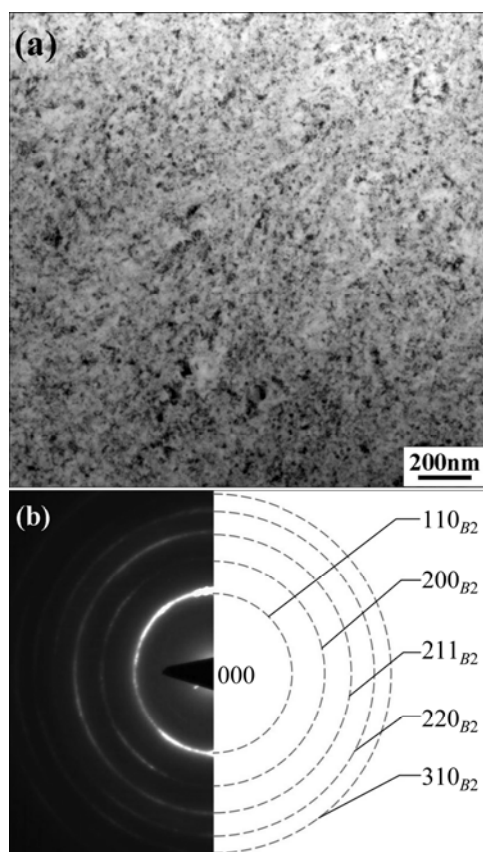


Fig. 4 Crystallization of NiTi sample subjected to SPD after annealing at 573 K for 2 h: (a) TEM bright-field image showing homogeneous nanocrystalline structure; (b) SAED pattern showing $B2$ austenite structure

3.4 Microstructures of amorphous NiTi sample after annealing at 723 K

Figure 5 shows the TEM image and the corresponding SAED pattern of microstructure of NiTi sample subjected to SPD and subsequent annealing at 723 K for 2 h. Annealing at 723 K for 2 h also leads to the complete nanocrystallization of NiTi sample subjected to SPD. However, as compared with the NiTi sample annealed at 573 K, the counterpart annealed at 723 K possesses the larger grain size and the mean grain size is about 50 nm. The SAED pattern indicates that the nanocrystalline NiTi sample consists of plenty of $B2$ austenite and a small amount of $B19'$ martensite.

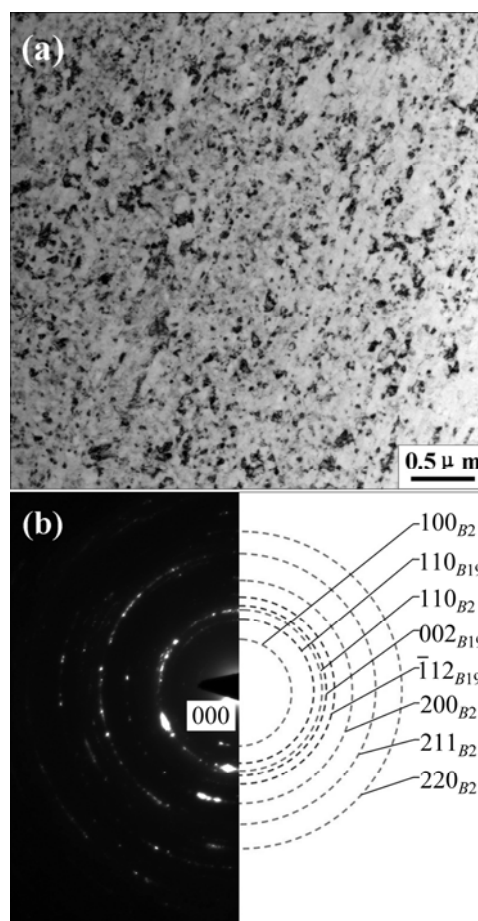


Fig. 5 Crystallization of NiTi sample subjected to SPD after annealing at 723 K for 2 h: (a) TEM bright-field image showing homogeneous nanocrystalline structure; (b) SAED pattern showing mixture of $B2$ austenite and $B19'$ martensite

3.5 Microstructures of amorphous NiTi sample after annealing at 873 K

Figure 6 indicates the TEM image and the corresponding SAED pattern of microstructure of NiTi sample subjected to SPD as well as subsequent annealing at 873 K for 2 h. It can be seen from Fig. 6(a) that the microstructure of the NiTi sample is characterized by the martensitic morphology as well as the coarse grains which are much larger than 200 nm, and in fact it is composed of $B19'$ martensite and $B2$ austenite. Furthermore, it can be observed from Fig. 6(b) that the substructure of the $B19'$ martensite contains a lot of dislocations and twins. The annealing twins belong to the (001) martensite compound twins, as shown in Figs. 6(c) and (d). In addition, the annealing twins distribute across the grain boundary and keep the consistent orientation relation against the grain boundary. It is possible that the grain boundary is an inherited consequence of the original grain boundary subjected to amorphization by SPD after being annealed at 873 K for 2 h.

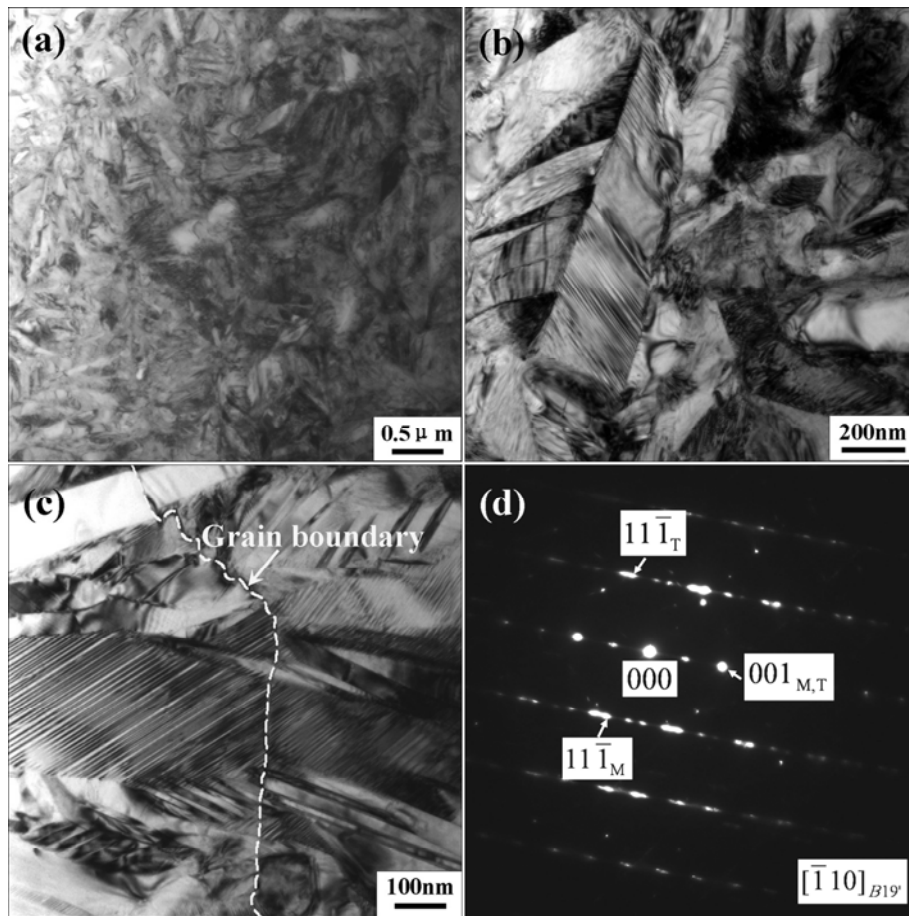


Fig. 6 Crystallization of NiTi sample subjected to SPD after annealing at 873 K for 2 h: (a) TEM bright-field image showing martensite morphology; (b) TEM bright-field image showing substructure of dislocations and twins; (c) TEM bright-field image showing morphology of annealing twins; (d) SAED pattern of twins in (c) showing (001) martensite compound twins

4 Discussion

The crystallization of the amorphous NiTi alloy can be regarded as a nucleation and growth process, which is dependent on the annealing temperature and the annealing time. In the case of isothermal atmosphere, the crystallization of the amorphous NiTi alloy can be mathematically described by the following Johnson–Mehl–Avrami–Kolmogorov (JMAK) equation [20–22]:

$$x=1-\exp(-kt^n) \quad (1)$$

where x is the volume fraction crystallized; t is the crystallization time; n is the Avrami exponent, which reflects the characteristic of nucleation and growth during crystallization; k is a temperature-dependent constant, which can be expressed by the following Arrhenius equation:

$$k = k_0 \exp\left(-\frac{Q}{RT}\right) \quad (2)$$

where k_0 is a constant; Q is activation energy; R is the mole gas constant; T is the thermodynamic temperature.

The following expression can be obtained by taking the logarithm of Eq. (1) twice.

$$\ln[-\ln(1-x)] = \ln k + n \ln t \quad (3)$$

A plot of $\ln[-\ln(1-x)]$ versus $\ln t$ can be used for determining the kinetic parameters k and n , where k is derived from the intercept ($\ln k$) of the plot and n is obtained by the slope of the plot. In general, n ranges from 1 to 2 for one-dimensional growth, from 2 to 3 for two-dimensional growth and from 3 to 4 for three-dimensional growth [23]. In the present study, it is difficult to accurately determine the kinetic parameters k , n and Q , which will be investigated in the future. However, the JMAK theory lays the foundation for better understanding the crystallization behavior of the amorphous NiTi sample in the case of the different annealing temperatures.

According to the JMAK theory, the nucleation rate and the growth rate of the amorphous NiTi sample during crystallization increase with the increase in the annealing temperatures. In the case of the onset of full crystallization, namely when all the crystallized grains

impinge each other, annealing at 873 K leads to the minimum time, and annealing at 573 K leads to the maximum time, while annealing at 723 K results in the intermediate time, which are schematically described in Fig. 7. In addition, it can be assumed that the nucleation rate is greater than the growth rate during crystallization of the amorphous NiTi sample. Therefore, in the case of the onset of full crystallization, the average grain size will decrease with the increase of the annealing temperatures, and the corresponding experimental evidence will be investigated in the future work. However, it can be found from the experimental results obtained at present that the average grain size of the NiTi sample annealed at 573 K is the minimum, but the average grain size of the NiTi sample annealed at 873 K is the maximum. The phenomenon reveals that the annealing time of 2 h is far greater than the time taken in the case of the onset of full crystallization, so the crystallized grains after full crystallization merge and grow each other with the progression of the annealing time. In fact, SPD of NiTi alloy based on local canning compression leads to a mixture of amorphous and nanocrystalline phases. Physical mechanism of crystallization of amorphous and nanocrystalline NiTi alloy subjected to SPD is attributed to the two procedures, namely the preferential nucleation and growth of the retained nanocrystalline debris, and then the nucleation and the growth of the amorphous matrix [16]. The overall crystallization process of the NiTi sample subjected to SPD can be outlined in Fig. 8. It can be seen from Fig. 8 that the retained nanocrystalline debris preferentially nucleates in the case of thermal driving force, where the stored energy in the retained nanocrystalline debris due to a high density of dislocations will be released to facilitate the occurrence of the crystal nucleus. With the progression of the annealing time, the retained nanocrystalline crystals continue to grow up, while the new crystal nuclei arise in the amorphous matrix due to the relaxation of the stored energy based on the lattice defects of the amorphous phase. When all the grains impinge each other, the NiTi sample subjected to SPD is completely crystallized. With the further increase in the annealing time, the fine grains are merged into the coarse grains, compared with the

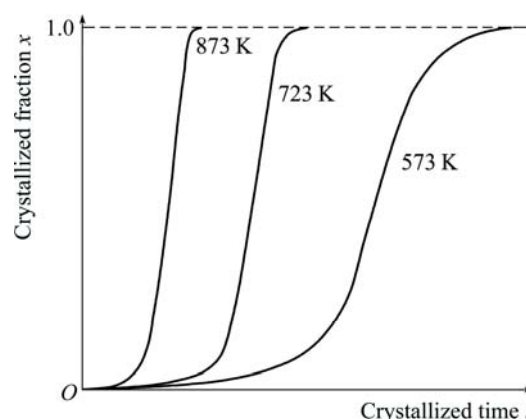


Fig. 7 Schematic diagram of crystallized fraction and grain size as function of crystallized time

coarse grains, the fine grains possess higher grain boundary energy.

It can be found from Figs. 4–6 that in the case of different annealing temperatures, the annealed NiTi samples exhibit the different grain sizes, and they possess the different phase structures as well. The phenomenon demonstrates that the grain size after crystallization has a significant influence on the martensite transformation of NiTi SMA. For example, in the nanocrystalline NiTi alloy subjected to annealing at 573 K for 2 h, the martensite transformation is suppressed with the decrease in the grain size. However, as compared with the original NiTi alloy prior to SPD, the crystallized NiTi sample subjected to SPD and annealing at 723 K for 2 h exhibits the higher martensite start transformation temperature M_s in the large nanocrystalline grains. In particular, the coarse-grained NiTi sample annealed at 873 K for 2 h has a considerable increase in the martensite start transformation temperature M_s , and thus facilitates the martensite phase transformation, in which (001) compound twins arise in order to compensate the transformation shape strain and decrease the strain energy [14,15]. However, (001) compound twin does not give a solution to the phenomenological crystallographic theory and cannot be a lattice invariant shear, so it is recognized as a deformation twin [24–26]. It is concluded that in the NiTi sample obtained by crystallization of the

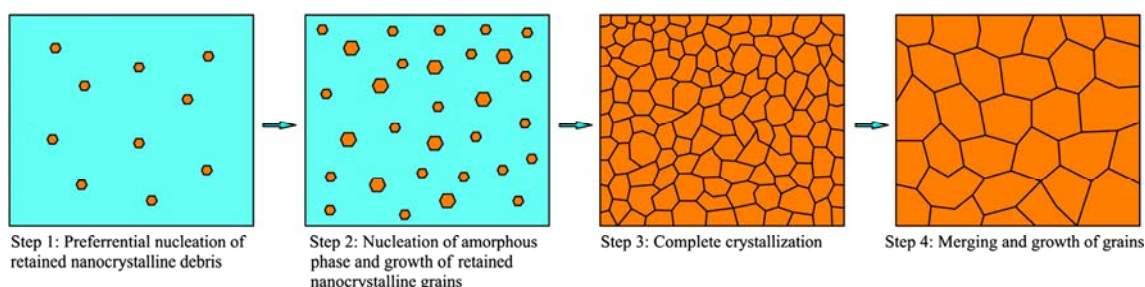


Fig. 8 Schematic diagram of crystallization process of amorphous NiTi sample subjected to SPD

amorphous phase, the (001) compound twin occurs more frequently instead of $\{111\}$ type I twin and $\langle 011 \rangle$ type II twin.

According to the above investigations, it can be concluded that the martensite phase transformation is suppressed with the decrease in the grain size in the nanocrystalline NiTi sample. The suppression of martensite phase transformation due to the decrease in the grain size was also reported in the case of nanocrystalline NiTi alloy subjected to HPT and subsequent annealing [14]. It is generally accepted that martensite nucleates more easily at the dislocation tangles and at the grain boundaries. As for the crystallized NiTi alloy, the NiTi sample with the nanocrystalline grains possesses less dislocation defects, while the NiTi sample with the coarse grains possesses more dislocation defects. It can be evident from Fig. 6 that plenty of dislocations exist in the microstructures of the annealed NiTi sample with the coarse grains, since the formation of the coarse grains is attributed to merging and growth of the nanocrystalline grains, which leads to the occurrence of a lot of dislocation defects. It seems that the dislocations arise more frequently at the grain boundaries, which contributes to the nucleation of martensite phase. It can be obviously found from Fig. 6(c) that the martensitic twins nucleate at the grain boundary at the beginning and they grow up towards the two different grains. In addition, grain refinement plays a significant role in suppressing the martensitic phase transformation, since the nucleation of martensite is impeded due to the constraint of the grain boundaries.

5 Conclusions

1) SPD based on local canning compression is capable of preparing the almost complete amorphous NiTi alloy, in which a small amount of retained nanocrystalline phases are embedded in the amorphous matrix. Furthermore, the B2 austenite phase and the B19' martensite phase coexist in the retained nanocrystalline debris. SPD can lead to the occurrence of stress-induced martensite phase transformation as well as mechanical stabilization of stress-induced martensite.

2) The amorphous NiTi structure induced by SPD can be subjected to complete crystallization by means of the appropriate heat treatment. The crystallization kinetics of the amorphous NiTi alloy can be mathematically described by the Johnson–Mehl–Avrami–Kolmogorov (JMAK) equation. The crystallization of the amorphous NiTi sample belongs to a nucleation and growth process, where the retained nanocrystalline debris acts as a preferential nucleus, which is attributed to the relaxation of the stored energy based on the dislocation defects.

3) Annealing at 573 K and 723 K leads to the complete nanocrystallization of the amorphous NiTi sample induced as a result of SPD. Martensitic phase transformation is suppressed in the nanocrystalline NiTi sample, where the nucleation of martensite is impeded due to the constraint of the grain boundaries. Crystallization of the amorphous NiTi sample annealed at 873 K leads to the occurrence of the coarse grains, where martensitic phase transformation occurs more easily and the annealing twins are observed. The annealing twins are determined as (001) martensite compound twins as well as the deformation twins. Furthermore, it can be found that the martensitic twins nucleate at the grain boundary.

References

- [1] OTUKA K, REN X. Physical metallurgy of Ti–Ni-based shape memory alloys [J]. Progress in Materials Science, 2005, 50(5): 511–678.
- [2] JIANG S Y, ZHANG Y Q. Microstructure evolution and deformation behavior of as-cast NiTi shape memory alloy under compression [J]. Transactions of Nonferrous Metals Society of China, 2012, 22(1): 90–96
- [3] CHROBAK D, STRÓŻ D. Two-stage *R* phase transformation in a cold-rolled and annealed Ti–50.6 at.%Ni alloy [J]. Scripta Materialia, 2005, 52(8): 757–760.
- [4] MITWALLY M E, FARAG M. Effect of cold work and annealing on the structure and characteristics of NiTi alloy [J]. Materials Science and Engineering A, 2009, 519: 155–166.
- [5] KHMELEVSKAYA I Y, PROKOSHKIN S D, DOBATKIN S V, TATYANIN E V, TRUBITSYNA I B. Studies of composition, deformation temperature and pressure effects on structure formation in severely deformed TiNi-based alloys [J]. Materials Science and Engineering A, 2006, 438–440: 472–475.
- [6] KIM Y H, CHO G B, HUR S G, JEONG S S, NAM T H. Nanocrystallization of a Ti–50.0Ni(at.%) alloy by cold working and stress/strain behavior [J]. Materials Science and Engineering A, 2006, 438–440: 531–535.
- [7] PETERLECHNER M, WAITZ T, KARNTHALER H P. Nanoscale amorphization of severely deformed NiTi shape memory alloys [J]. Scripta Materialia, 2009, 60(12): 1137–1140.
- [8] TSUCHIYA K, INUZUKA M, TOMUS D, HOSOKAWA A, NAKAYAMA H, MORII K, TODAKA Y, UMEMOTO M. Martensitic transformation in nanostructured TiNi shape memory alloy formed via severe plastic deformation [J]. Materials Science and Engineering A, 2006, 438–440: 643–648.
- [9] TSUCHIYA K, HADA Y, KOYANO T, NAKAJIMA K, OHNUMA M, KOIKE T, TODAKA Y, UMEMOTO M. Production of TiNi amorphous/nanocrystalline wires with high strength and elastic modulus by severe cold drawing [J]. Scripta Materialia, 2009, 60(9): 749–752.
- [10] ZHENG Y F, HUANG B M, ZHANG J X, ZHAO L C. The microstructure and linear superelasticity of cold-drawn TiNi alloy [J]. Materials Science and Engineering A, 2001, 279: 25–35.
- [11] SERGUEEVA A V, SONG C, VALIEV R Z, MUKHERJEE A K. Structure and properties of amorphous and nanocrystalline NiTi prepared by severe plastic deformation and annealing [J]. Materials Science and Engineering A, 2003, 339: 159–165.
- [12] DELVILLE R, MALARD B, PILCH J, SITTNER P, SCHRYVERS D. Microstructure changes during non-conventional heat treatment of

- thin Ni–Ti wires by pulsed electric current studied by transmission electron microscopy [J]. *Acta Materialia*, 2010, 58(13): 4503–4515.
- [13] MALARD B, PILCH J, SITTNER P, DELVILLE R, CURFS C. In situ investigation of the fast microstructure evolution during electropulse treatment of cold drawn NiTi wires [J]. *Acta Materialia*, 2011, 59(4): 1542–1556.
- [14] NAKAYAMA H, TSUCHIYA K, UMEMOTO M. Crystal refinement and amorphisation by cold rolling in TiNi shape memory alloys [J]. *Scripta Materialia*, 2001, 44(8–9): 1781–1785.
- [15] WAITZ T, KAZYKHANOV V, KARNTHALER H P. Martensitic phase transformations in nanocrystalline NiTi studied by TEM [J]. *Acta Materialia*, 2004, 52(1): 137–147.
- [16] WAITZ T. The self-accommodated morphology of martensite in nanocrystalline NiTi shape memory alloys [J]. *Acta Materialia*, 2005, 53(8): 2273–2283.
- [17] SRIVASTAVA A K, YANG Z Q, SCHRYVERS D, HUMBEECK J V. Effect of annealing on cold-rolled Ni–Ti alloys [J]. *Materials Science and Engineering A*, 2008, 481–482: 594–597.
- [18] PETERLECHNER M, BOKELOH J, WILDE G, WAITZ T. Study of relaxation and crystallization kinetics of NiTi made amorphous by repeated cold rolling [J]. *Acta Materialia*, 2010, 58(20): 6637–6648.
- [19] JIANG S Y, ZHANG Y Q, ZHAO L H, ZHENG Y F. Influence of annealing on NiTi shape memory alloy subjected to severe plastic deformation [J]. *Intermetallics*, 2013, 32: 344–351.
- [20] LI J J, WANG J C, XU Q, YANG G C. Comparison of Johnson–Mehl–Avrami–Kologoromov (JMAK) kinetics with a phase field simulation for polycrystalline solidification [J]. *Acta Materialia*, 2007, 55(3): 825–832.
- [21] TODINOV M T. On some limitations of the Johnson–Mehl–Avrami–Kolmogorov equation [J]. *Acta Materialia*, 2000, 48(17): 4217–4224.
- [22] LIU K T, DUH J G. Kinetics of the crystallization in amorphous NiTi thin films [J]. *Journal of Non-Crystalline Solids*, 2007, 353(11–12): 1060–1064.
- [23] KALU P N, WARYOBA D R. A JMAK-microhardness model for quantifying the kinetics of restoration mechanisms in inhomogeneous microstructure [J]. *Materials Science and Engineering A*, 2007, 464: 68–75.
- [24] KNOWLES K M, SMITH D A. The crystallography of the martensitic transformation in equiatomic nickel-titanium [J]. *Acta Materialia*, 1981, 29(1): 101–110.
- [25] ONDA T, BANDO Y, OHBA T, OTSUKA K. Electron microscopy study of twins in martensite in a Ti–50.0 at% Ni alloy [J]. *Materials Transactions, JIM*, 1992, 33(4): 354–359.
- [26] LIU Y, XIE Z L, VAN HUMBEECK J, DELAEY L. Asymmetry of stress–strain curves under tension and compression for NiTi shape memory alloys [J]. *Acta Materialia*, 1998, 46(12): 4325–4338.

大塑性变形制备的非晶镍钛形状记忆合金的晶化

江树勇¹, 唐明¹, 赵亚楠¹, 胡励², 张艳秋¹, 梁玉龙²

1. 哈尔滨工程大学 工程训练中心, 哈尔滨 150001;

2. 哈尔滨工程大学 材料科学与化学工程学院, 哈尔滨 150001

摘要: 局部包套压缩大塑性变形能够实现镍钛形状记忆合金的完全非晶化, 其中少量残留的纳米晶相分布在非晶基体上。研究非晶镍钛合金在 573、723 和 873 K 退火条件下的晶化机制。采用约翰逊–迈尔方程描述非晶镍钛合金的晶化动力学行为。在 573 和 723 K 的退火条件下, 可以获得具有完全纳米晶相的镍钛形状记忆合金, 在该纳米晶镍钛形状记忆合金中, 马氏体相变由于晶界的约束而受到了抑制。在 873 K 的退火条件下, 非晶镍钛合金的晶化产生了晶粒粗大的镍钛形状记忆合金样品。在室温条件下的粗晶镍钛样品中, 可以观察到马氏体复合孪晶, 而且发现马氏体孪晶在晶界优先形核, 并且向两个不同的晶粒内部长大。局部包套压缩大塑性变形结合后续退火工艺为制备纳米晶镍钛形状记忆合金提供了一种新的途径。

关键词: 镍钛合金; 形状记忆合金; 大塑性变形; 非晶化; 晶化

(Edited by Xiang-qun LI)